Searches for scalar resonances with di-photon in association with leptons and taus using the easyjet analysis framework in ATLAS detector at the LHC

Kutlwano Makgetha[1,2], Vuyolwethu Kakancu[1,2], Njokweni Mbuyiswa[1,2], Kgothatso Ntumbe[1,2], Paballo Ndhlovu[1,2], Phuti Rapheeha[2,3], Reda Mekouar[4], Mukesh Kumar[1], Rachid Mazini[1] and Bruce Mellado[1,2]

[1]School of Physics and Institute for Collider Particle Physics, University of the Witwatersrand, Johannesburg, Wits 2050, South Africa
[2]iThemba LABS, National Research Foundation, PO Box 722, Somerset West 7129, South Africa
[3]School of Electrical Engineering, Tshwane University of Technology, Staatsartillerie Road, Pretoria West 0001, South Africa
[4]Institute of High Energy Physics, Beijing, University of Chinese Academy of Sciences, 19B Yuquan Road, Shijingshan District, Beijing, China

E-mail: 2134657@students.wits.ac.za

Abstract. Recent studies have identified growing excesses in scalar resonances with di-photon at the Large Hadron Collider (LHC), suggesting the presence of scalar particles beyond the Standard Model. These scalar resonances are motivated by the multi-lepton anomalies at the LHC which indicate a potential new scalar particle S with a mass of approximately 152 GeV, originating from a heavier scalar H, with a global significance of $\sim 5\sigma$. Motivated by these findings, the HBSM group within the HMBS physics group at ATLAS has launched a new analysis using the easyjet analysis framework. This analysis focuses on searching for scalar resonances through di-photon production in the process $gg \to H \to SS'$, where $S \to \gamma\gamma$ and S' decays to $S' \to \tau_h\tau_\ell$. We are preparing to use the analysis tools to analyse the 2022-2024 Run 3 data with an integrated luminosity of 35.7 fb^{-1} at $\sqrt{s} = 13.6$ TeV.

1 Introduction

The Standard Model (SM) is the foundational theoretical framework that describes elementary particles and three of the four fundamental forces: electromagnetic, strong, and weak interactions [1–3]. It categorises particles into two main groups: fermions, which have a spin of $\frac{1}{2}$, and bosons, which have integer spins. Fermions, including quarks and leptons, are the fundamental constituents of matter, while bosons act as force carriers that mediate interaction between fermions. Key examples of bosons include photons (which mediate the electromagnetic force), gluons (which mediate the strong force), and the $W^{\pm}$ and Z bosons (which mediate the weak force). Despite its successes, the SM has limitations, including multi-lepton anomalies observed at the LHC. These anomalies, which include excesses in dilepton and trilepton events (with and without b-jets), align with multiple ATLAS and CMS observations where SM backgrounds are expected to dominate. A potential explanation for these excesses involves a heavier scalar resonance H decaying into lighter scalars S and S' (mass $m_S \approx 150 \pm 5$ GeV) [4–11]. The Two-Higgs Doublet Model with a scalar singlet (S) [12] is a minimal extension of the SM that addresses experimental phenomena, such as the excess of diphoton events at the LHC. In this model, the Higgs-like scalar S decays to electroweak bosons ($\gamma\gamma$, WW^*, ZZ^*), yielding final states rich in leptons, photons, and missing transverse energy.

Indirect searches of LHC data have revealed a narrow resonance at $m_S = 152$ GeV in diphoton and $Z\gamma$ invariant mass spectra, with $\sim 5\sigma$ global significance [13], corroborating previous findings [14,15]. While the S' production mechanism remains unclear, data suggests its association with $H \to SS'$, and the decay chain $H \to SS'$ followed by $S \to WW^*$ further explains the observed lepton-rich anomalies.

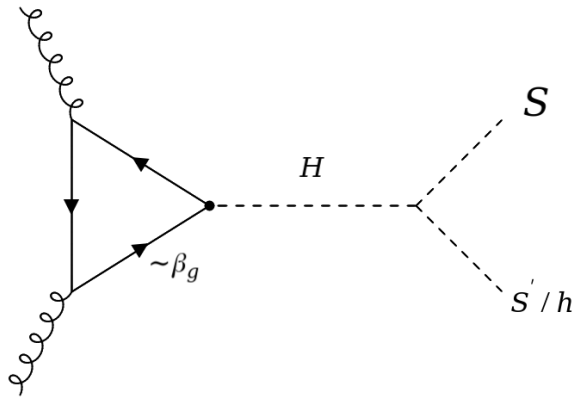

Figure 1: Feynman diagram for the $X \to H \to SS'$ decay.

2 Data Analysis

As outlined in the abstract, these are the proposed final states for the entire analysis $S' \to \tau_h\tau_\ell$, $S' \to \ell + b$ (where $\ell = e, \mu, \tau$), $S' \to 2(\ell, \tau, b)$, but the focus in this proceeding will be on the semileptonic ($\tau_h\tau_\ell$) and 1-tau (τ) category. We are conducting this analysis using the easyjet analysis framework [16] with the 2022-2024 ATLAS run 3 data with an integrated luminosity of 35.7 fb^{-1} at $\sqrt{s} = 13.6$ TeV. This preliminary work uses Monte Carlo (MC) simulations with pile-up profiles matching 2022 data; however, the completed analysis will look at the full Run 3 data.

2.1 ATLAS Detector

The ATLAS experiment is one of the two general purpose detectors at the LHC, aimed at exploring a broad spectrum of physics, from validating the SM to searching for new physics. With over 5500 scientists from 245 institutions across 42 countries, ATLAS is one of the largest scientific projects globally. The detector measures 25 m in diameter, 44 m in length, and weighs around 7000 tonnes (7000000 kg). Its design accommodates the detection of critical signals for new physics while enduring a harsh radiation environment. ATLAS's capability to measure particle properties with precision is enhanced by its nearly full 4π solid angle coverage, allowing for the reconstruction of most physics processes. This includes the study of the Higgs boson production and decay, and searches for BSM physics. The detector is designed to withstand radiation damage and includes robust cooling and 26 magnetic field generation systems to ensure optimal performance.

2.2 Simulation Details and Filters

We use the $\gamma\gamma$ML analysis package in the easyjet analysis framework as it already has our desired final states and is well defined. We study the diphoton production with top quark pairs ($\gamma\gamma t\bar{t}$) as one of our dominant backgrounds because top quarks decay into W bosons and b quarks, with W bosons further decaying into a charged lepton and missing transverse energy.

2.3 Object Selections

Tau leptons decay via 1-prong and 3-prong topological modes. A 1-prong τ decays into one charged hadron (such as a pion) along with neutrinos, resulting in a single track in the detector and missing energy. A 3-prong τ, on the other hand, decays into three charged hadrons (typically pions) and a neutrino, producing a more complex but distit signature with three visible tracks. In this work, we are only interested in the visible hadronic tau (τ_h) candidates as tau leptons decay before reaching the detector. To identify τ_h candidates, we used different levels of selection criteria known as working points (WP), which can be classified as loose, medium, and tight. We used the Recurrent Neural Network (RNN) loose identification because we want to include more τ_h candidates, aiming to maximise signal efficiency, even if it means accepting more background [17, 18]. Specifically, RNN was used because taus

decay into multiple particles (prongs), and their decay products form a sequence of tracks that can be modeled sequentially. RNNs are good at capturing dependencies in sequences. We selected the Medium Deep Neural Network (DNN) LooseVarRad electron WP to ensure detector stability and balance efficiency with background rejection. Electron classification is performed using DNN. For the muon, we used the MediumPflowLooseVarRad WP to improve muon identification by combining information from the muon spectrometer to reconstruct particles more precisely and keep a relatively high efficiency for the muons. All photon selections use the loose WP, except where explicitly stated otherwise in the trigger name (e.g., medium or tight) [19]. Taus, electrons, and photons are excluded from the transition region ($1.37 < |\eta| < 1.52$) due to the overlapping geometric coverage and changing detector characteristics between the barrel and endcap subdetectors. This region presents reconstruction challenges as particles may traverse gaps or boundaries between detector components, such as the electromagnetic calorimeters, leading to reduced precision in tracking and energy measurements. Muon reconstruction relies on the muon spectrometer, which extends to higher pseudorapidity and doesn't exhibit the same transition effects. The pseudorapity ($|\eta| < 2.5$) cut ensures reliable particle reconstruction within the detector's well-instrumented region, beyond which tracking, calorimeter, and trigger performance degrade due to reduced silicon tracker coverage and detector acceptance. The diphoton triggers listed in the table are carefully designed to balance signal efficiency and background rejection, taking into account pile-up effects and optimizing for different experimental conditions. The use of varying energy thresholds, identification criteria, and Level-1 requirements ensures that the triggers are versatile and robust, capable of capturing a wide range of diphoton events while minimising noise. The following table lists the diphoton trigger chains used in the analysis for the years 2022 and 2023.

Table 1: Diphoton Trigger Chains by Year.

Year	**Trigger Chains**
2022	HLT_2g50_loose_L12EM20VH HLT_g35_medium_g25_medium_L12EM20VH HLT_2g22_tight_L12EM15VHI
2023	HLT_2g50_loose_L12eEM24L HLT_g35_medium_g25_medium_L12eEM24L HLT_g45_medium_g20_medium_L1eEM40L_2eEM18L HLT_2g22_tight_L12eEM18M

Table 2: Selection criteria for different particle types.

Selection Criterion	**Photons**	**Taus**	**Electrons**	**Muons**
Minimum Transverse Momentum (P_T)	25 GeV	25 GeV	10 GeV	10 GeV
Maximum Pseudorapidity (η)	2.37	2.5	2.5	2.5
Identification	Loose	RNN	MediumDNN	MediumPFlow
Isolation Requirement	Non-Isolated	Loose	LooseVarRad	LooseVarRad

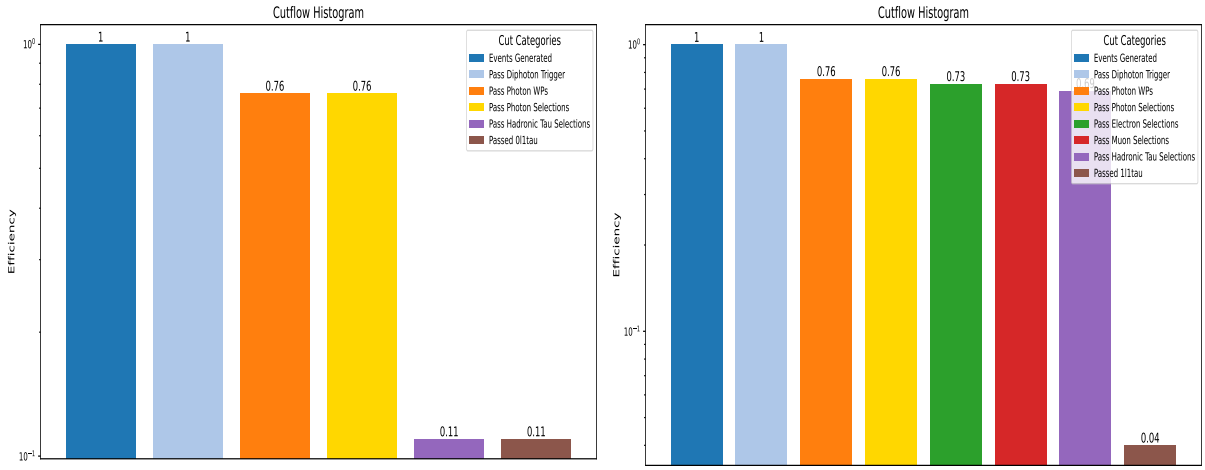

Figure 2: Cutflow histogram for the $0\ell 1\tau$ (left) and $1\ell 1\tau$ (right) final states.

3 Preliminary Results

In this section, we present the kinematic distributions from our background sample ($\gamma\gamma t\bar{t}$), where we defined two final states as stated above. For simplicity, we chose to show the multiplicity (indicating the number of objects in our final states), transverse momentum, and pseudorapidity distributions because that is where we applied our object selections.

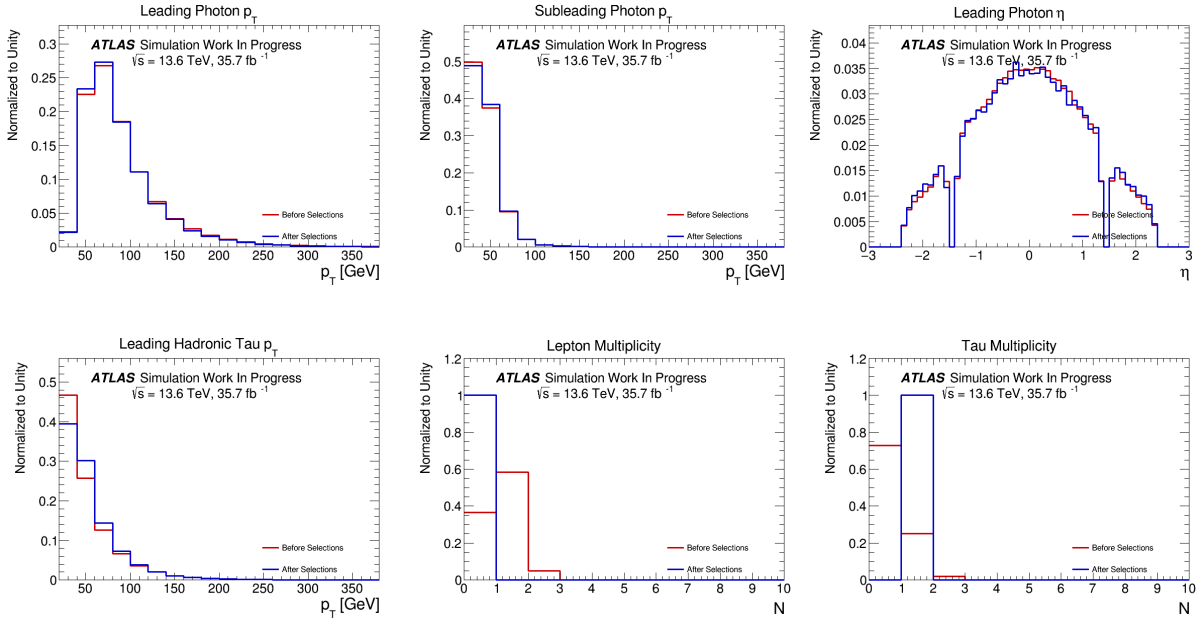

Figure 3: Selected kinematics for the $0\ell 1\tau$ final state.

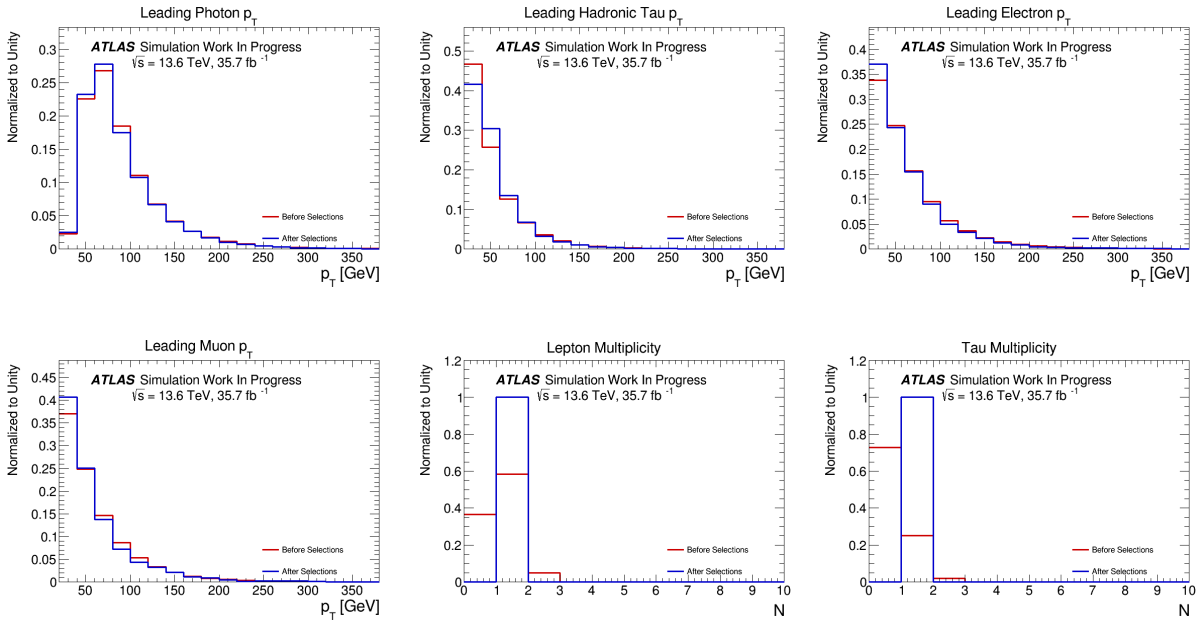

Figure 4: Selected kinematics for $1\ell 1\tau$ final state.

4 Conclusion and Future Plans

We have requested full MC production for the $\gamma\gamma\tau^+\tau^-$ signal and its mass scans, and are preparing a similar request for the dilepton and one lepton final states at $\sqrt{s} = 13.6$ TeV. Object selections for the dominant $\gamma\gamma t\bar{t}$ background are complete. We are currently studying the $V\gamma\gamma$ background, applying the object selection methods described in this paper. Upon receiving the $\gamma\gamma\tau^+\tau^-$ signal samples, we will incorporate them into our analysis. We will then characterise the background by comparing 2D sideband and TMVA methods for estimating background events in the signal region, subtracting this estimate from the data to isolate the signal. These data-driven methods reduce systematic uncertainties compared to MC simulations by minimising reliance on accurate simulation of detector effects and backgrounds, and are extendable to higher dimensions. For signal, we used Madgraph5@NLO for matrix element calculations and Pythia8 for parton showering and hadronisation. Events were generated using AthGeneration release 23.6.23 to produce an EVNT file. Truth-level information was obtained using Athena release 25.0.9 and the derivation_tf.py algorithm to output a TRUTH1 level root file. The gluon-gluon fusion (ggF) is the production mode, and systematic uncertainties are included in the ggF process. We have requested 120000 events. The following table summarises the simulation setup for different scalar masses and cross-sections:

Table 3: Simulation Parameters for Tau Channel ($X \to H \to SS' \to \gamma\gamma\tau^+\tau^-$)

DSID	H Mass (GeV)	S Mass (GeV)	S' Mass (GeV)	Cross-sections (fb)	Events
562134	250	150	95	1.154	120000
562135	260	160	100	0.412	120000
562136	300	175	125	0.053	120000
562137	350	225	125	0.010	120000
562138	400	275	125	0.004	120000

5 Acknowledgments

I would like to express my gratitude to the SA-CERN Excellence bursary for funding this research.

References

[1] G. Altarelli, "The standard model of particle physics," *arXiv preprint hep-ph/0510281*, 2005.

[2] G. Kane, *Modern elementary particle physics: explaining and extending the standard model*. Cambridge University Press, 2017.

[3] R. L. Workman *et al.*, "Review of Particle Physics," *PTEP*, vol. 2022, p. 083C01, 2022.

[4] S. von Buddenbrock, A. S. Cornell, A. Fadol, M. Kumar, B. Mellado, and X. Ruan, "Multi-lepton signatures of additional scalar bosons beyond the Standard Model at the LHC," *J. Phys. G*, vol. 45, no. 11, p. 115003, 2018.

[5] S. Buddenbrock, A. S. Cornell, Y. Fang, A. Fadol Mohammed, M. Kumar, B. Mellado, and K. G. Tomiwa, "The emergence of multi-lepton anomalies at the LHC and their compatibility with new physics at the EW scale," *JHEP*, vol. 10, p. 157, 2019.

[6] S. von Buddenbrock, R. Ruiz, and B. Mellado, "Anatomy of inclusive $t\bar{t}W$ production at hadron colliders," *Phys. Lett. B*, vol. 811, p. 135964, 2020.

[7] Y. Hernandez, M. Kumar, A. S. Cornell, S.-E. Dahbi, Y. Fang, B. Lieberman, B. Mellado, K. Monnakgotla, X. Ruan, and S. Xin, "The anomalous production of multi-lepton and its impact on the measurement of Wh production at the LHC," *Eur. Phys. J. C*, vol. 81, no. 4, p. 365, 2021.

[8] A. Crivellin and B. Mellado, "Anomalies in particle physics and their implications for physics beyond the standard model," *Nature Rev. Phys.*, vol. 6, no. 5, pp. 294–309, 2024.

[9] A. Crivellin, Y. Fang, O. Fischer, S. Bhattacharya, M. Kumar, E. Malwa, B. Mellado, N. Rapheeha, X. Ruan, and Q. Sha, "Accumulating evidence for the associated production of a new Higgs boson at the LHC," *Phys. Rev. D*, vol. 108, no. 11, p. 115031, 2023.

[10] S. Bhattacharya, B. Lieberman, M. Kumar, A. Crivellin, Y. Fang, R. Mazini, and B. Mellado, "Emerging Excess Consistent with a Narrow Resonance at 152 GeV in High-Energy Proton-Proton Collisions," 3 2025.

[11] G. Coloretti, A. Crivellin, S. Bhattacharya, and B. Mellado, "Searching for low-mass resonances decaying into W bosons," *Phys. Rev. D*, vol. 108, no. 3, p. 035026, 2023.

[12] S. von Buddenbrock, N. Chakrabarty, A. S. Cornell, D. Kar, M. Kumar, T. Mandal, B. Mellado, B. Mukhopadhyaya, R. G. Reed, and X. Ruan, "Phenomenological signatures of additional scalar bosons at the LHC," *Eur. Phys. J. C*, vol. 76, no. 10, p. 580, 2016.

[13] S. Von Buddenbrock, A. S. Cornell, E. D. Iarilala, M. Kumar, B. Mellado, X. Ruan, and E. M. Shrif, "Constraints on a 2hdm with a singlet scalar and implications in the search for heavy bosons at the lhc," *Journal of Physics G: Nuclear and Particle Physics*, vol. 46, no. 11, p. 115001, 2019.

[14] A.-T. Mulaudzi, M. Kumar, A. Goyal, and B. Mellado, "Constraining 2hdm+ s model through w-boson mass measurements," *arXiv preprint arXiv:2312.08807*, 2023.

[15] A. Crivellin and B. Mellado, "Anomalies in particle physics and their implications for physics beyond the standard model," *Nature Reviews Physics*, vol. 6, no. 5, pp. 294–309, 2024.

[16] EASYjet Team, "easyjet: an athanalysis physics-analysis framework (runs 2 3)," https://gitlab.cern.ch/easyjet/easyjet, Jan. 2022, cERN GitLab repository; created January 19, 2022; Apache License 2.0; 1 668 commits, 6 branches, 46 tags, 7 releases.

[17] A. Collaboration *et al.*, "Identification of hadronic tau lepton decays using neural networks in the atlas experiment," ATL-PHYS-PUB-2019-033, Tech. Rep., 2019.

[18] G. Aad, B. Abbott, J. Abdallah, S. Abdel Khalek, O. Abdinov, R. Aben, B. Abi, M. Abolins, O. S. AbouZeid, H. Abramowicz *et al.*, "Identification and energy calibration of hadronically decaying tau leptons with the atlas experiment in pp collisions at s= 8 tev," *The European Physical Journal C*, vol. 75, no. 7, p. 303, 2015.

[19] A. Collaboration *et al.*, "Electron and photon performance measurements with the atlas detector using the 2015-2017 lhc proton-proton collision data," *arXiv preprint arXiv:1908.00005*, 2019.